# Supporting Information

## 1. Experimental Section

### 1.1 Preparation of materials

*Preparation of Co-$MnO_2|O_v$ and $MnO_2$*: 0.395 g (2.5 mmol) potassium permanganate ($KMnO_4$) and 0.169 g (1 mmol) manganese (II) sulfate monohydrate ($MnSO_4 \cdot H_2O$) were dissolved in 40 ml deionized water with continuous stirring for 1 h, followed by addition of 0.135 g cobaltous chloride ($CoCl_4 \cdot 6H_2O$, mass ratio of $CoCl_4 \cdot 6H_2O/MnSO_4 \cdot H_2O$ was 0.8) and stirring for another 1 h. The solution was transferred into a 50 mL Teflon-lined autoclave and heated at 160 °C for 12 h. After cooled down to room temperature, the Co-$MnO_2|O_v$ was washed with distilled water several times and freeze dried for 12 h. Preparation of $MnO_2$ was similar with the Co-$MnO_2|O_v$, but without $CoCl_4 \cdot 6H_2O$ in the mixture solution.

*Preparation of Mn/Co-N-C and Mn-N-C:* 1g as-prepared Co-$MnO_2|O_v$ was dispersed in 250 ml 1 M HCl solution. Then 1.5 ml aniline was added dropwise under continuous stirring in an ice bath (temperature below 5 ℃). The solution was further stirred for 6 h, and the product was centrifuged, cleaned by deionized water several times (until the PH value was about 7) and freeze dried for 12 h. The obtained polyaniline was pyrolyzed at 900 ℃ for 3 h with 5 ℃/min under Ar atmosphere, followed by acid washing with 0.5 M $H_2SO_4$ solution at 80 ℃ for 5 h and cleaning with deionized water. After that, freeze drying was performed to get Mn/Co-N-C sample. The Mn-N-C sample was prepared similarly as above, the only difference being Co-$MnO_2|O_v$ replaced by $MnO_2$.

### 1.2 Separator modification

The Mn/Co-N-C or Mn-N-C modified separator was fabricated by vacuum filtration method. The modifying material, CNTs and polyvinylidene difluoride (PVDF) were mixed with a mass ratio of 8:1:1, and dispersed in isopropyl alcohol and

ultrasonicated for 30 min. After that, the suspension was vacuum-filtered on commercial polypropylene separator (Celgard 2324) and dried for 5 h. The modified separator was cut into circular disks with diameter of 16 mm and catalyst mass loading of 0.6 mg $cm^{-2}$.

### 1.3 Preparation of sulfur cathode

In a typical procedure, 25 wt% BP-2000 and 75 wt% commercial sulfur were ground completely. The resultant mixture was heated at 155 ℃ for 12 h, and collected after cooling to room temperature. Next, 70 wt% active material (BP-2000/S), 20 wt% Super P and 10 wt% PVDF were mixed with 1-methyl-2-pyrrolidinone (NMP) to form a homogeneous slurry. The slurry was coated onto an aluminum foil current collector and dried at 60 ℃ for 12 h. Finally, the cathode was cut into circular pieces with diameter of 12 mm. The sulfur loading was about 1 mg $cm^{-2}$.

For high sulfur loading, the sulfur and Ketjen Black (mass ratio was 85:15) were ground completely and heated at 155 ℃ for 12 h. The product was mixed with Super P and PVDF (mass ratio being 8:1:1) in NMP and stirred for 12 h. The resulting slurry was coated on an aluminum foam current collector and dried at 60 ℃. The loading mass of sulfur was controlled by the concentration of slurry.

### 1.4 Materials characterization

The microstructures and elemental distribution of the samples were obtained on a Tecnai G2F30 STWIN Transmission Electron Microscope (TEM) and a Nova Nano SEM 450 Scanning Electron Microscope (SEM) equipped with energy dispersive X-ray spectroscopy (EDS). High angle annular dark-field (HAADF) images were taken on a Titan ETTEM Themis microscope operating at 300 kV with a spherical aberration corrector. X-ray diffraction (XRD) tests were carried out on a Lab XRD-7000s advance diffractometer with 2θ range of 10°-90°. Raman spectra were recorded on a in Via instrument with a 532 nm laser excitation. X-ray photoelectron spectroscopy (XPS) was taken on an ESCALAB250Xi spectrophotometer. Inductively coupled plasma mass spectroscopy (ICP-MS) was recorded on an Agilent 7900 instrument. Electron spin

resonance (ESR) spectra were used to explore active oxygen vacancies ($O_{vac}$) on a Bruker EMXnano equipment. The surface area and pore size distribution were measured using the BET theory and Langmuir models (Autosorb-IQ-C).

### 1.5 Battery assembling

The Li-S batteries were assembled as RC2016-type coin cells in a glove box filled with highly pure Ar atmosphere. As-prepared sulfur composite, modified separator and lithium metal were used as cathode, separator and anode, respectively. The electrolyte was prepared by adding 0.1 M $LiNO_3$ additive to 1 M bis(trifluoromethane) sulfonamide lithium within dimethoxyethane and dioxolane (1:1, v/v) mixed solvent. The amount of electrolyte injected into each side of separator was 15 μL $mg^{-1}$.

The symmetric cell was assembled with active material as the working and counter electrodes. The active material was mixed with PVDF binder (mass ratio being 9:1) in N-Methylpyrrolidone (NMP) to form a slurry and coated onto the aluminum foil. The resulting electrode sheet was cut into circular disks of 12 mm diameter with active material loading of around 0.6 mg $cm^{-2}$. The electrolyte was 0.2 M $Li_2S_6$ solution; the amount of electrolyte injected into each side of separator was 20 μL.

### 1.6 Electrochemical measurements

The cycling performance and rate performance of Li-S cells were investigated on a LAND testing system between 1.7 and 2.8 V (vs. $Li^+/Li$) at different current densities. Cyclic voltammetry (CV) and electrochemical impedance spectroscopy (EIS) tests were carried out on CHI608D electrochemical workstation. CV of Li-S batteries were tested at a scan rate of 0.1 to 0.4 mV $s^{-1}$ between 1.7-2.8 V. The symmetric cells were tested at scan rates of 0.2, 5 and 50 mV $s^{-1}$ between -1.0-1.0 V. EIS tests were conducted from 0.01 Hz to 100 kHz with a voltage amplitude of 5 mV.

### 1.7 Lithium sulfide deposition tests

A $Li_2S_8$ solution (0.2 mol $L^{-1}$) was used as the electrolyte and synthesized by mixing lithium sulfide and sulfur powder (molar ratio was 1:7) in tetraglyme under

vigorous magnetic stirring for 24 h. Aluminum foil loaded with 0.8 mg $cm^{-2}$ catalyst was used as cathode, and lithium foil was used as the anode. 25 μL $Li_2S_8$ electrolyte was added into the cathode and 20 μL electrolyte without $Li_2S_8$ was dropped on the anode. The batteries were galvanostatically discharged to 2.10 V at 0.10 mA and maintained potentiostatically at 2.05 V until the current dropped below $10^{-5}$ A. After that, the lithium sulfide deposited and grew on the electrode surface.

### 1.8 Theoretical calculations

Density of states and partial density of states values for the Mn-N-C and Mn/Co-N-C as well as the adsorption of $Li_2S_6$ on Mn-N-C and Mn/Co-N-C were calculated based on density functional theory (DFT) using the Cambridge Sequential Total Energy Package program in the Materials Studio package. The generalized gradient approximation with a Perdew–Burke–Ernzerhof function and Grimme method for the DFT-D correlation were utilized to describe the electronic exchange and correlation effects. Moreover, the plane-wave cutoff was tested and set to 500 eV. The self-consistent field tolerance was $2 \times 10^{-6}$ eV with the on-the-fly generated (OTFG) ultrasoft pseudo-potential for core electrons and the electronic minimizer of All Bands/EDFT.

### 1.9 Lithium ion transference number ($t_{Li}^+$) and ionic conductivity

The $t_{Li}^+$ was recorded with chronoamperometry at a voltage step of 10 mV on an electrochemical working station. The cell was assembled by sandwiching a modified separator between two Li metal pieces in a CR2016 coin cell. The following equation was used to estimate the $Li^+$ transference number.

$$t_{Li}^+ = I_s/I_o$$

Where $t_{Li}^+$ designates the $Li^+$ transference number, $I_s$ describes the steady state current, and $I_o$ is the initial state current.

The ionic conductivity was determined by EIS analysis with a frequency from $10^5$ to $10^{-2}$ Hz and an amplitude of 5 mV. The following equation was used to calculate the ionic conductivity.

$$\sigma = \frac{L}{R \times A}$$

Where σ is the ionic conductivity, R represents the bulk resistance of the separator, L and A are the separator's thickness and area, respectively.

## 2. Results and discussion

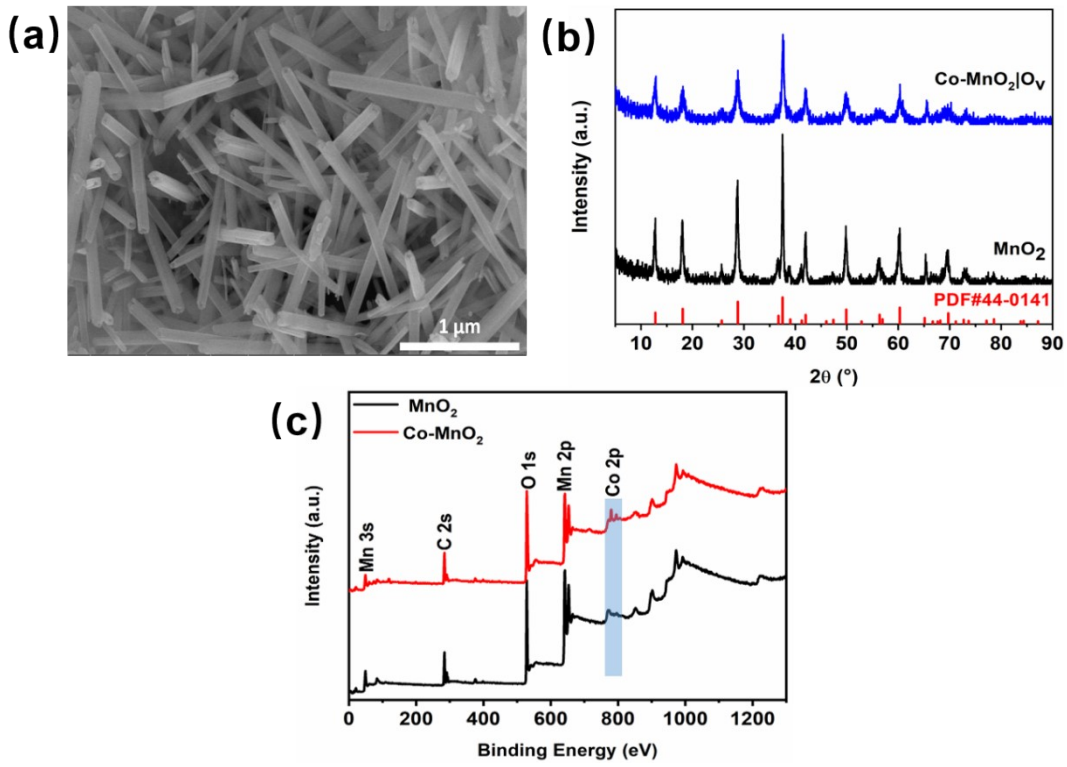


Figure S1. (a) SEM image of $MnO_2$. (b) XRD patterns and (c) XPS survey spectra of $MnO_2$ and Co-dope $MnO_2$.

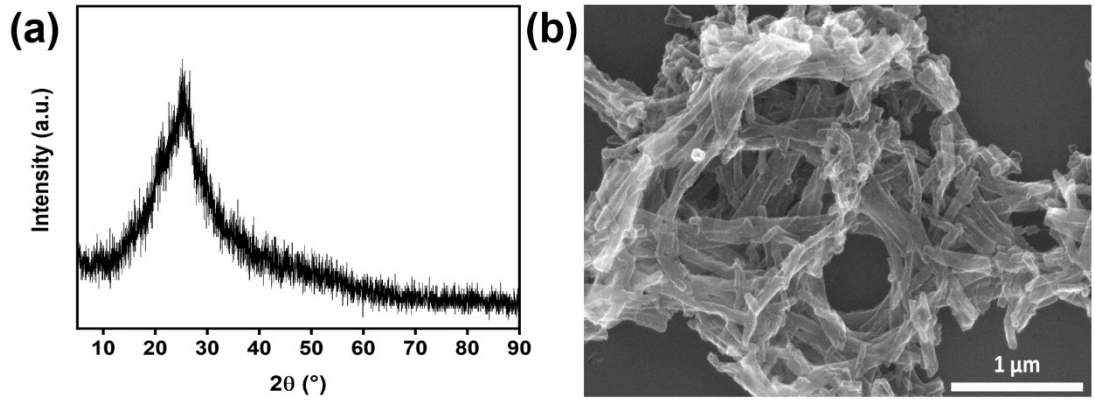


Figure S2. (a) XRD pattern and (b) SEM image of PANI.

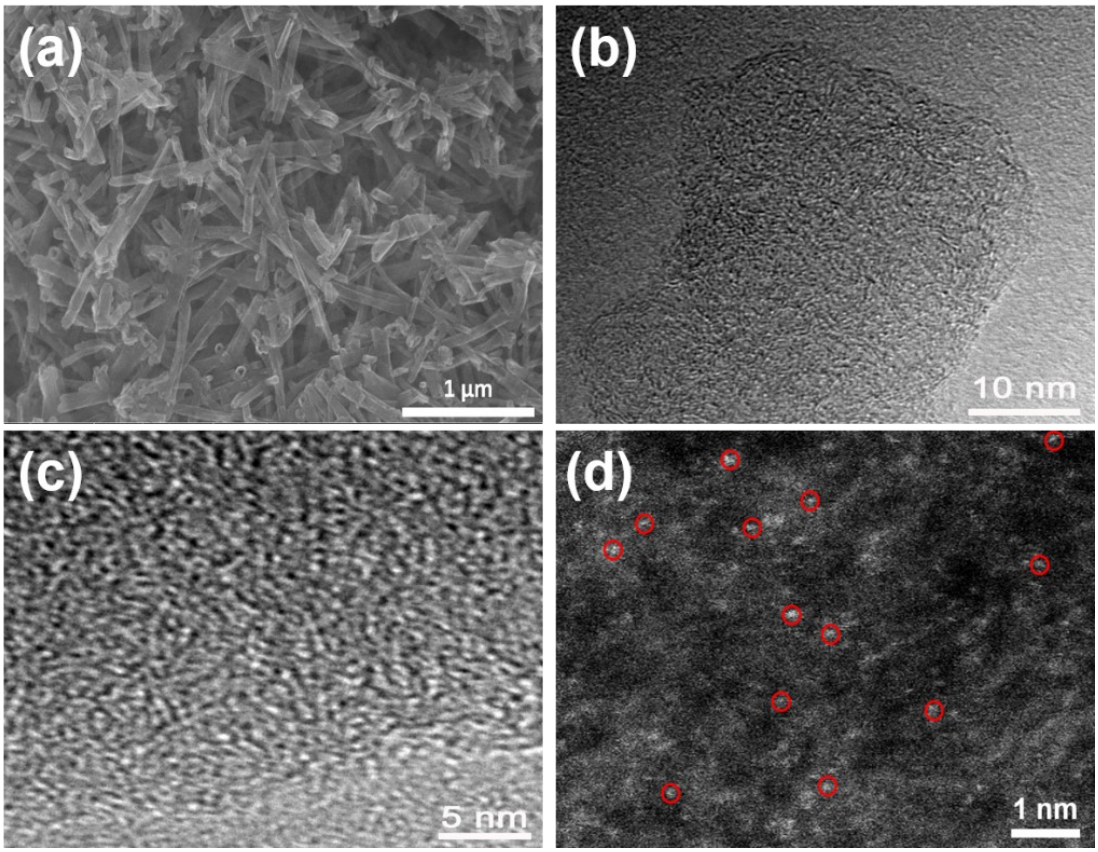


Figure S3. (a) SEM image of Mn-N-C catalyst. (b) TEM and (c) high-resolution TEM images of Mn/Co-N-C catalyst. (d) Aberration-corrected HAADF-STEM of Mn-N-C catalyst.

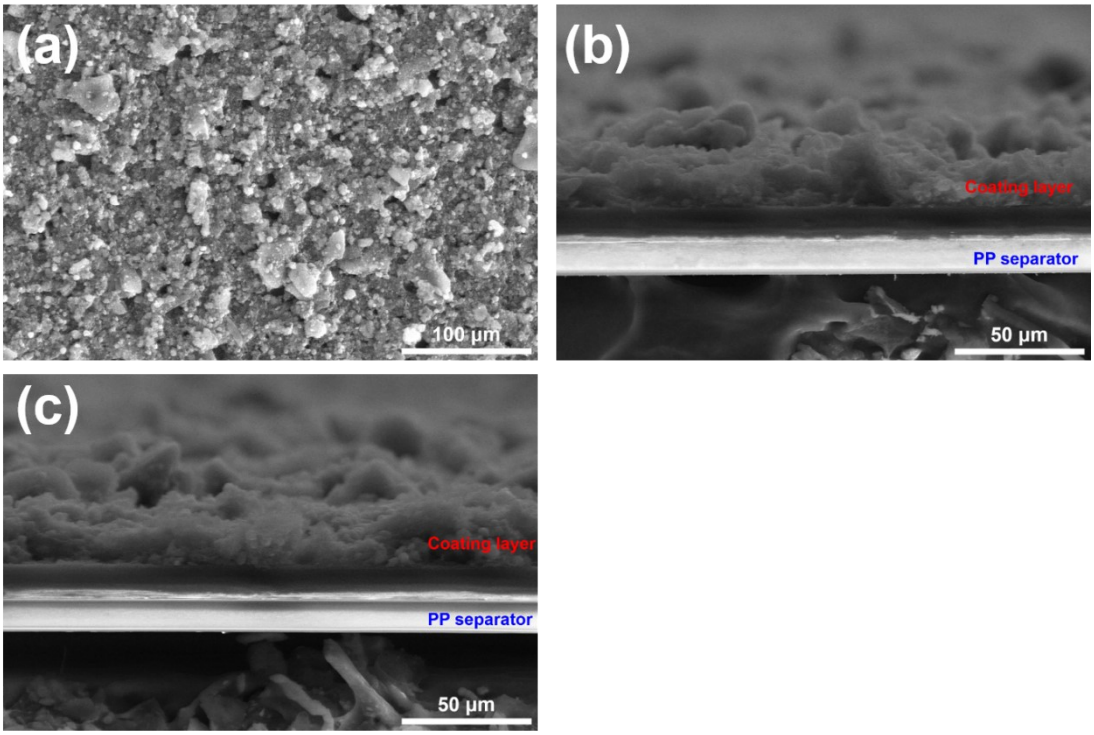


Figure S4. (a, b) Surface- and cross-sectional SEM images of Mn-N-C modified separator. (c) cross-sectional SEM image of Mn/Co-N-C modified separator.

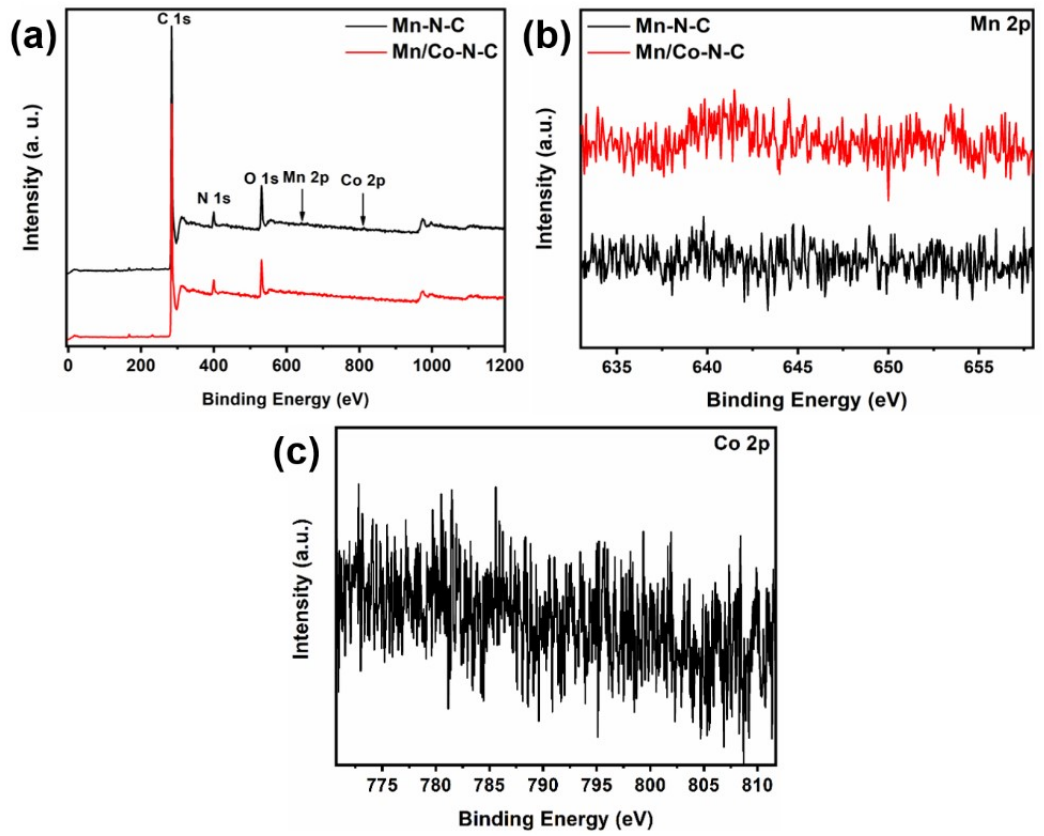


Figure S5. (a) XPS survey spectra and (b) Mn 2p of Mn/Co-N-C and Mn-N-C. (c) Co 2p XPS of Mn/Co-N-C.

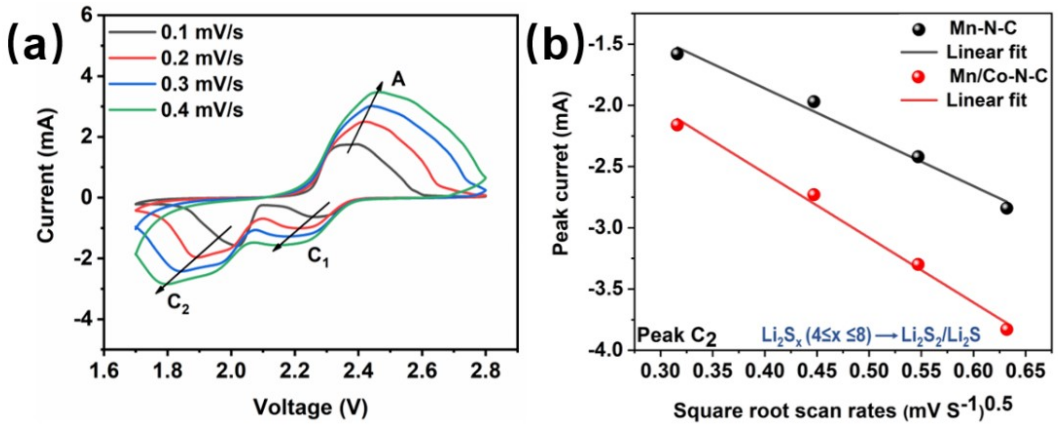


Figure S6. (a) CV curves of Mn-N-C cell at scan rates from 0.1 mV $s^{-1}$ to 0.4mV $s^{-1}$. (b) CV peak current versus the square root of the scan rates based on peak C2 of CV.

Table S1. Comparison of $Li^+$ diffusion coefficients

| Separator | Mn-N-C | Mn/Co-N-C |
|---|---|---|
| $D_{Li}^+$ at peak A ($cm^2\ s^{-1}$) | $5.97\times10^{-10}$ | $8.45\times10^{-10}$ |
| $D_{Li}^+$ at peak $C_1$ ($cm^2\ s^{-1}$) | $1.11\times10^{-8}$ | $1.45\times10^{-8}$ |
| $D_{Li}^+$ at peak $C_2$ ($cm^2\ s^{-1}$) | $7.28\times10^{-10}$ | $1.33\times10^{-9}$ |

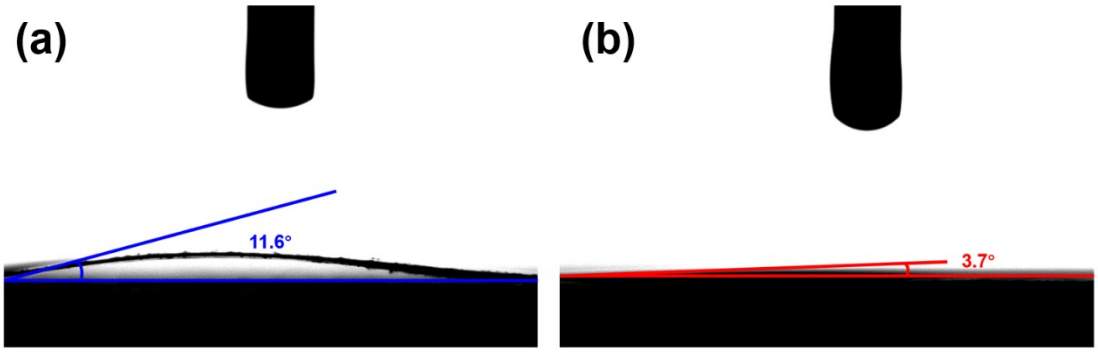


Figure S7. The electrolyte contact angle of (a) Mn-N-C and (b) Mn/Co-N-C catalysts modified separator.

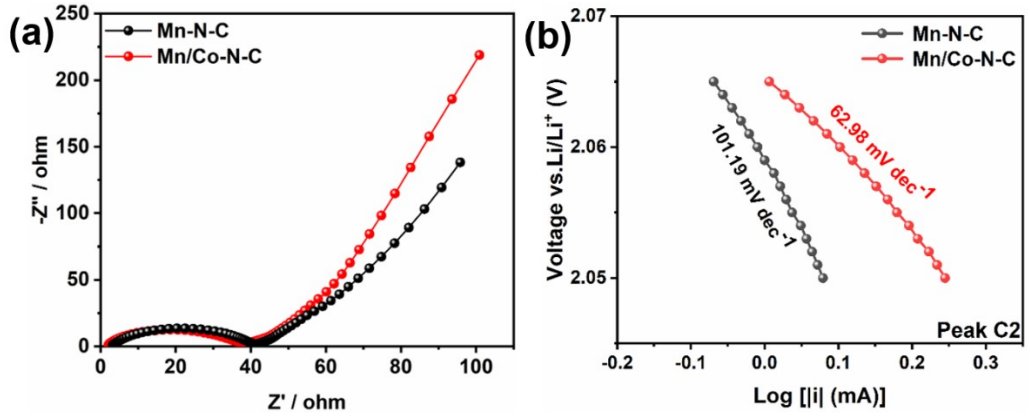


Figure S8. (a) EIS curves of the Li-S cells with different separators. (b) Tafel plots based on Peak C2 of different separators.

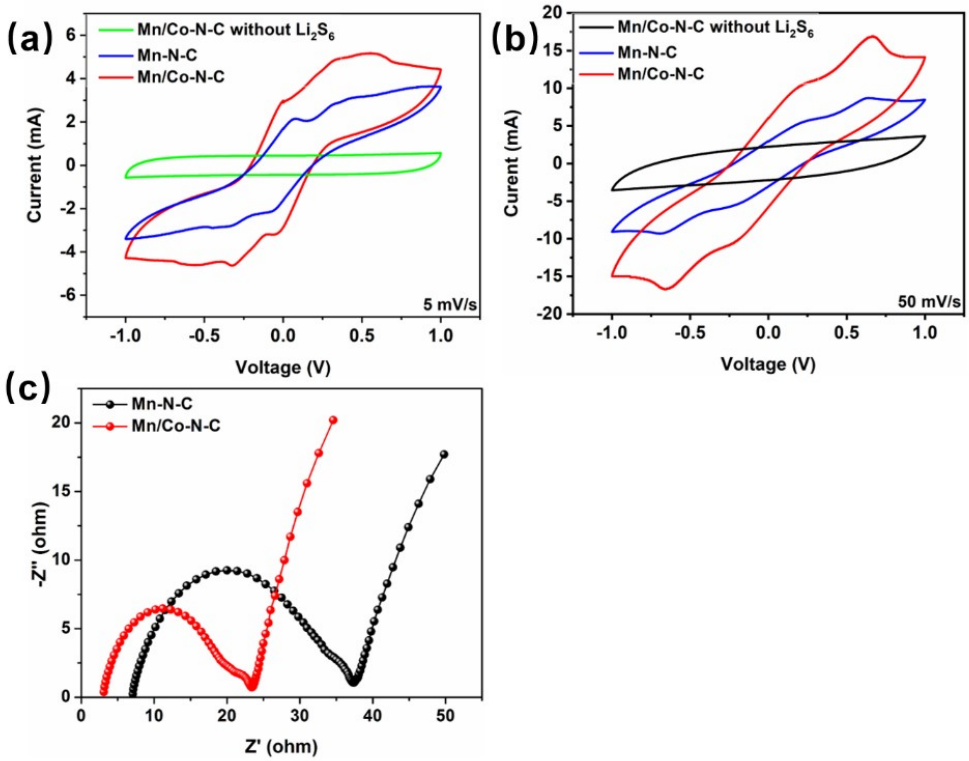


Figure S9. (a, b) CV profiles of the symmetrical cells at 5 mV $s^{-1}$ and 50 mV $s^{-1}$. (c) EIS spectra of symmetrical cells.

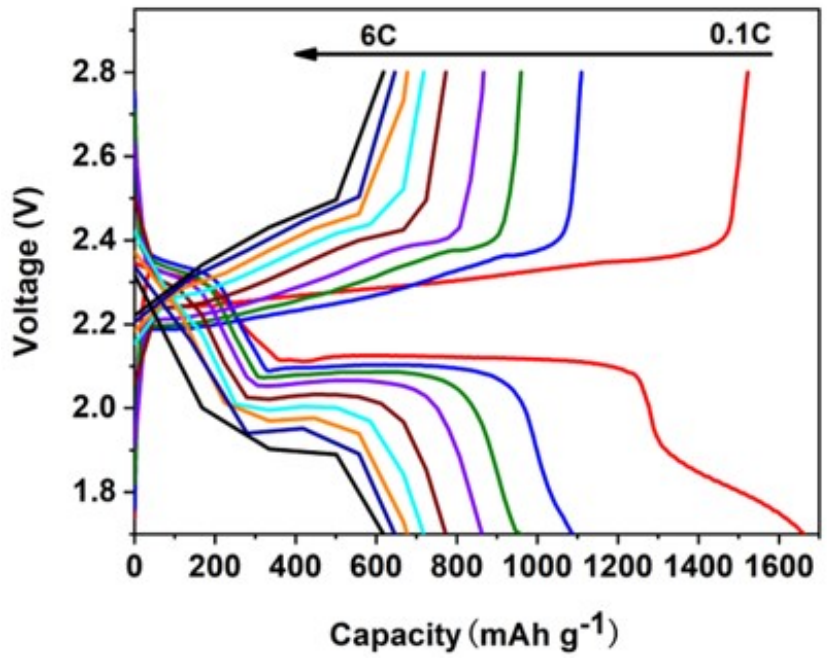


Figure S10. (a) Charge/discharge profiles of Li-S battery with Mn/Co-N-C at different current densities.

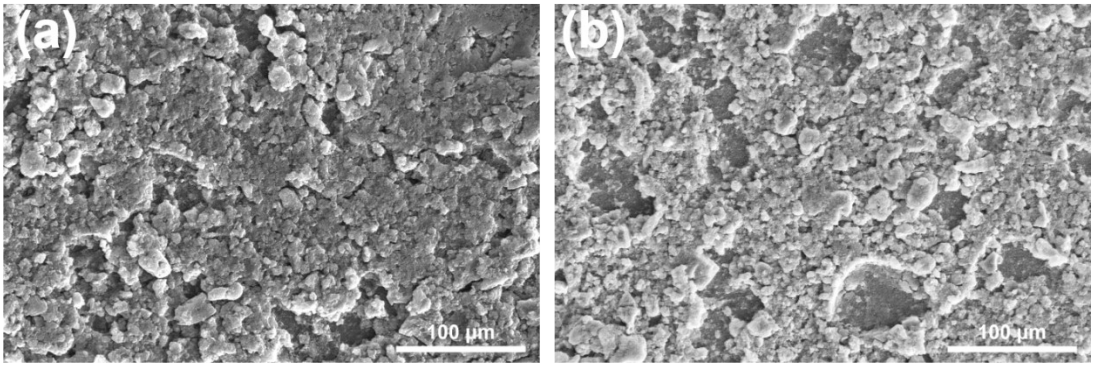


Figure S11. SEM images of (a) Mn-N-C and (b) Mn/Co-N-C modified separators after cycling.

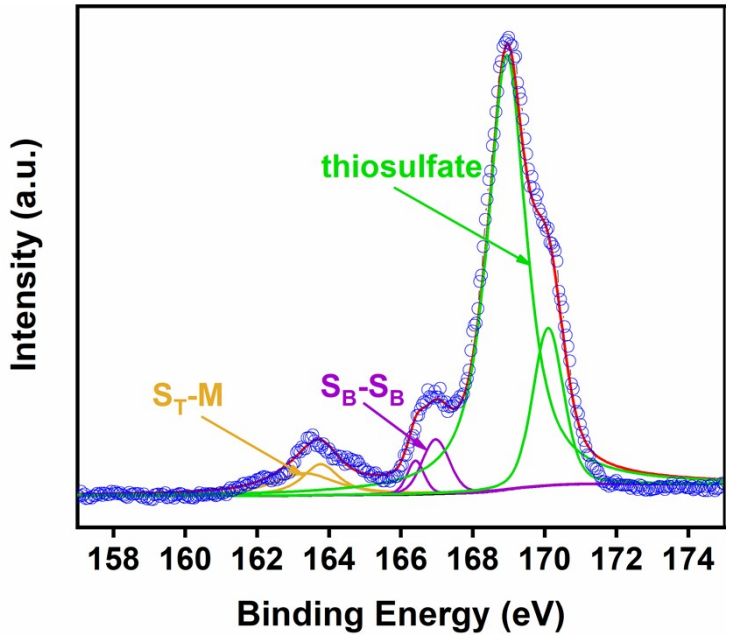


Figure S12. S 2p XPS spectra of Mn/Co-N-C modified separators after cycling.

Table S2 Comparison of electrochemical properties of various catalyst for Li–S batteries.

| **Composites** | **S content (mg/cm$^2$)** | **Discharge capacity (mAh/g)** | **Cycle performance** | | | **Ref.** |
|---|---|---|---|---|---|---|
| | | | Capacity decay per cycle (%) | Current density (C) | Cycle number | |
| **Co−N/G** | 2.0 | 1210 (0.2 C)<br>618 (4 C) | 0.053 | 1 | 500 | [1] |
| **CNT@SACo** | 1.0 | 1496 (0.1 C)<br>641 (2 C) | 0.064 | 1 | 500 | [2] |
| **HFeNG** | 2.0 | 1298 (0.2 C)<br>810 (5 C) | 0.083 | 0.5 | 300 | [3] |
| **Ni@NG** | 1.0 | 1598 (0.2 C)<br>612 (10 C) | 0.06 | 10 | 500 | [4] |

| | | | | | | |
|---|---|---|---|---|---|---|
| **B/2D MOF-Co** | 1.5 | 1138 (0.1 C)<br>478 (5C) | 0.07 | 1 | 600 | [5] |
| **Co-NG** | 0.5-1.0 | 648 (6 C) | 0.08 | 0.5 | 600 | [6] |
| **Zn-HNC** | 1.0 | 989 (10 C) | 0.015 | 5 | 700 | [7] |
| **Co-N/KB** | 3.0 | 905 (0.2 C)<br>629 (1 C) | 0.025 | 0.5 | 200 | [8] |
| **CoSA-N-C** | 1.2 | 1307 (0.1 C)<br>829 (2 C) | 0.035 | 1 | 1000 | [9] |
| **Co-PCNF** | 3.5 | 965 (0.1 C)<br>617 (1 C) | 0.082 | 0.2 | 600 | [10] |
| **Co−N/G** | 2.0 | 1210 (0.2 C)<br>618 (4 C) | 0.053 | 1 | 500 | [11] |
| **C-C-N-Co** | 1.0 | 1160 (0.1 C)<br>582 (5 C) | 0.058 | 2 | 700 | [12] |
| **SAZ-AF** | 1.5 | 1651 (0.1 C)<br>701 (5 C) | 0.05 | 2 | 1000 | [13] |
| **FeNSC** | 1.0 | 1306 (0.05 C)<br>550 (4 C) | 0.047 | 1 | 1000 | [14] |
| **SA-Fe/Fe2N@NG** | 1.5 | 1457 (0.1 C)<br>904 (4 C) | 0.033 | 1 | 500 | [15] |
| **Mn/Co-N-C** | **1.0** | 1662 (0.1 C)<br>625 (6 C) | **0.036** | **2** | **1000** | **This work** |

## Reference


[1] Z. Du, X. Chen, W. Hu, C. Chuang, S. Xie, A. Hu, W. Yan, X. Kong, X. Wu, H. Ji, L.J. Wan, J Am Chem Soc, 2019, 141, 3977-3985.

[2] Q. Lin, B. Ding, S. Chen, P. Li, Z. Li, Y. Shi, H. Dou, X. Zhang, ACS Appl Energ Mater, 2020, 3, 11206-11212.

[3] Y. Wang, D. Adekoya, J. Sun, T. Tang, H. Qiu, L. Xu, S. Zhang, Y. Hou, Adv Funct Mater, 2018, 29.

[4] L. Zhang, D. Liu, Z. Muhammad, F. Wan, W. Xie, Y. Wang, L. Song, Z. Niu, J. Chen, Adv Mater, 2019, 31, e1903955.

[5] Y. Li, S. Lin, D. Wang, T. Gao, J. Song, P. Zhou, Z. Xu, Z. Yang, N. Xiao, S. Guo, Adv Mater, 2020, 32, e1906722.

[6] X. Meng, X. Liu, X. Fan, X. Chen, S. Chen, Y. Meng, M. Wang, J. Zhou, S. Hong, L. Zheng, G. Shi, C.W. Bielawski, J. Geng, Adv Sci (Weinh), 2021, e2103773.

[7] H. Shi, X. Ren, J. Lu, C. Dong, J. Liu, Q. Yang, J. Chen, Z.S. Wu, Adv Energ Mater, 2020, 10.

[8] L. Jin, Z. Fu, X. Qian, F. Li, Y. Wang, B. Wang, X. Shen, Electrochim Acta, 2021, 382.

[9] Y. Li, J. Wu, B. Zhang, W. Wang, G. Zhang, Z.W. Seh, N. Zhang, J. Sun, L. Huang, J. Jiang, J. Zhou, Y. Sun, Energy Storage Mater, 2020, 30, 250-259.

[10] T. Huang, Y. Sun, J. Wu, J. Jin, C. Wei, Z. Shi, M. Wang, J. Cai, X.T. An, P. Wang, C. Su, Y.Y. Li, J. Sun, ACS Nano, 2021, 15, 14105-14115.

[11] Z. Du, X. Chen, W. Hu, C. Chuang, S. Xie, A. Hu, W. Yan, X. Kong, X. Wu, H. Ji, L.J. Wan, J Am Chem Soc, 2019, 141, 3977-3985.

[12] Y. Li, P. Zhou, H. Li, T. Gao, L. Zhou, Y. Zhang, N. Xiao, Z. Xia, L. Wang, Q. Zhang, L. Gu, S. Guo, Small Methods, 2020, 4.

[13] C.L. Song, Z.H. Li, L.Y. Ma, M.Z. Li, S. Huang, X.J. Hong, Y.P. Cai, Y.Q. Lan, ACS Nano, 2021.

[14] H. Zhao, B. Tian, C. Su, Y. Li, ACS Appl Mater Interfaces, 2021, 13, 7171-7177.

[15] C. Ma, Y. Zhang, Y. Feng, N. Wang, L. Zhou, C. Liang, L. Chen, Y. Lai, X. Ji, C. Yan, W. Wei, Adv Mater, 2021, e2100171.